Closed loop control of dielectric elastomer actuators based on self-sensing displacement feedback

IOP Publishing

Closed loop control of dielectric elastomer actuators based on self-sensing displacement feedback

Test
o

G Rizzello[1,2,3], D Naso[1], A York[2] and S Seelecke[2]

Abstract

This paper describes a sensorless control algorithm for a positioning system based on a dielectric elastomer actuator (DEA). The voltage applied to the membrane and the resulting current can be measured during the actuation and used to estimate its displacement, i.e., to perform self-sensing. The estimated displacement can be then used as a feedback signal for a position control algorithm, which results in a compact device capable of operating in closed loop control without the need for additional electromechanical or optical transducers. In this work, a circular DEA preloaded with a bi-stable spring is used as a case of study to validate the proposed control architecture. A comparison of the closed loop performance achieved using an accurate laser displacement sensor for feedback is also provided to better assess the performance limitations of the overall sensorless scheme.

Keywords: dielectric elastomer, dielectric elastomer actuator, DE, DEA, self-sensing, control, sensorless control

(Some figures may appear in colour only in the online journal)

1. Introduction

Dielectric elastomers (DEs), or dielectric electro-active polymers (DEAPs), represent a family of active materials which exhibit significant change in their size or shape as a consequence of the application of an external electric field. A DE consists of a thin elastomeric film (e.g. silicone or VHB acrylic) sandwiched between two compliant electrodes. When an electric field is applied to the DE, via a voltage at the electrode surface, the charges of opposite signs on the electrodes are attracted by electrostatic forces, generating a compression of the film and a consequent expansion of its area. Such an electrically induced deformation can be effectively used for actuation [1]. Large deformations, low power consumption, fast response time, high flexibility and low cost make DE actuators (DEA) a suitable alternative for the development of a new generation of devices such as pumps [2], valves [3], robots [4] and micropositioning stages [5]. On the other hand, DEAs exhibit creep and strong nonlinearities which tend to limit their dynamic performance when operating in open loop. The use of feedback control to compensate these effects is a viable solution to overcome such limits, enabling the use of DEA technology in a wider range of applications.

The major restriction of typical feedback control is the requirement of an external sensor for closing the loop. However, DEAs dual actuation-sensing capability allows for operation in closed loop without any external sensor, by exploiting the intrinsic feature of the material known as self-sensing [6]. When a DEA is actuated, its electrical impedance changes according to its geometry. If electrical measurements are performed while actuating, the materials electrical parameters can be estimated and used to reconstruct its deformation. Since electrical measurements, e.g. voltage

[3] Author to whom any correspondence should be addressed.

and current, are typically integrated in the circuit which drives the actuator, self-sensing can be potentially implemented without requiring any additional sensor. The concept of self-sensing, i.e. simultaneous sensing and actuation, represents a common feature of many active materials [7]. If the self-sensing signal is used as feedback for a position control algorithm, it allows the realization of a compact device which is able to actuate and sense at the same time, and operate in closed loop without the need of additional electro-mechanical transducers. This attractive concept is often referred to as 'self-sensing' control or 'sensorless' control.

The electrical dynamics of a DEA is characterized by high-voltage and low-current signals. In addition, there exists parasitic phenomena such as voltage drop on the electrodes and leakage current, making the implementation of self-sensing a nontrivial task. Several recent contributions report experimental investigation of self-sensing capabilities of DEA's. In [8], Chuc *et al* propose a force self-sensing technique for DEA's based on the electrical impedance measurement. The paper presents the concept and some preliminary experimental results. Jung *et al* describe in [9] a self-sensing methodology based on reconstructing the DEA capacitance from the output of a RC high-pass filter. The paper presents results at several actuation frequencies, but the proposed approach requires peak detectors which make the overall implementation more complex, and it also does not include the resistive effects of the electrodes. In [10], Matysek *et al* propose an electronic circuit capable to drive and sense up to eight DEA devices for a tactile display, in which the DEA self-sensing is performed by measuring the charge. In [11], Gisby *et al* propose a self-sensing algorithm which enables capacitance estimation and compensation of parasitic effects. The algorithm is based on a regression involving the DEA charge, voltage and current. Hoffstadt *et al* [12] propose an online identification algorithm based on a frequency domain approach which can be used for self-sensing. The algorithm requires voltage and current measurements only, as well as amplitude and phase information. They also discuss how the operating frequency affects the choice of the electrical model used to describe the DEA impedance.

The area of feedback control of DEA's has also gained increased attention in recent years. For instance, in [13] Sarban and Jones implement an adaptive control on a DEA based on a gray-box modeling approach. In [14], Wilson *et al* propose a cerebellar-inspired controller in applications where the DEA characteristics changes significantly. In [15], Rizzello *et al* investigate the limitations of model based PID control, and propose a modified controller consisting of a PID cascaded with a square root which performs a compensation of the main nonlinearity of the actuator. Despite its simple structure, this control scheme is particularly effective in dealing with DEA regulation, even when the actuator shows strong nonlinearities, i.e. hyper-elasticity and bi-stability [16, 17]. However, even though both self-sensing and feedback control have received considerable attention in recent years, only few works investigate the performance of self-sensing based closed loop control. A significant example is the work of Rosset *et al* [18], where the authors use the self-sensing approach in [11] within a closed loop PI control scheme. The implementation in [18] still has a number of unaddressed issues (e.g., no validation of the accuracy is provided, the PI is tuned for a specific operating point, and the closed loop bandwidth is relatively low), but the paper undoubtedly represents the first successful attempt to validate the sensor-free control loop scheme. Combining self-sensing with feedback control is in general a nontrivial operation, as the self-sensing tends to introduce delays in the feedback loop which may eventually produce destabilizing effects. Moreover, self-sensing feedback may introduce some additional undesirable effects such as amplification of measurement noise. In general, it is expected that a self-sensing control architecture leads to an overall decrease in performance with respect to a standard, sensor-based scheme, even if a quantitative measure of this decrease in performance has not been investigated yet, to the author's best knowledge. This paper moves in the same direction of the aforementioned work, by performing an experimental validation of a sensorless control scheme for a DEA, establishing both features and limitations of the proposed technique. In order to achieve sensorless control, we extend our previous work by combining the self-sensing algorithm proposed in preliminary conference paper [19] with the control approach described in [15]. The self-sensing technique aims at reconstructing the DEA capacitance and electrode resistance from voltage and current measurements by means of online identification algorithms. The methodology is based on a time-domain approach, and no specific hardware (e.g. PWM) is required for its implementation. The algorithm does not need any information on the DEA charge, and therefore it is not affected by drift due to the leakage current. Moreover, the algorithm has a relatively low computational complexity, as it consists of algebraic operations only (i.e. no peak or phase detections), so it can be operated in real time at fast rates (20 kHz in [19]). The selected controller structure is a PID cascaded with a square root, which was proven to be particularly effective for DEA set-point regulation and compensation of both material creep and nonlinearities [20]. A circular DEA membrane pre-loaded with a combination of a linear and a bi-stable spring is chosen as a case of study to validate the control architecture. The bi-stable biasing element allows to significantly increase the actuator stroke, at the cost of increasing the material nonlinearities. Several operative experiments are performed to assess the closed loop response of the DEA when the displacement feedback is provided by either an accurate laser displacement sensor or by the self-sensing algorithm.

The reminder of the paper is organized as follows. Section 2 illustrates the operating principle of the bi-stable DEA and discusses on modeling. Section 3 discusses the self-sensing algorithm and the overall sensorless control architecture, while section 4 summarizes the experimental validation campaign. Finally, section 5 provides conclusive remarks.

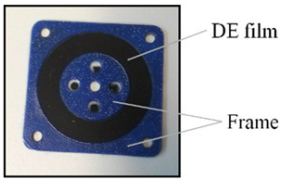

Figure 1. Circular DE Membrane.

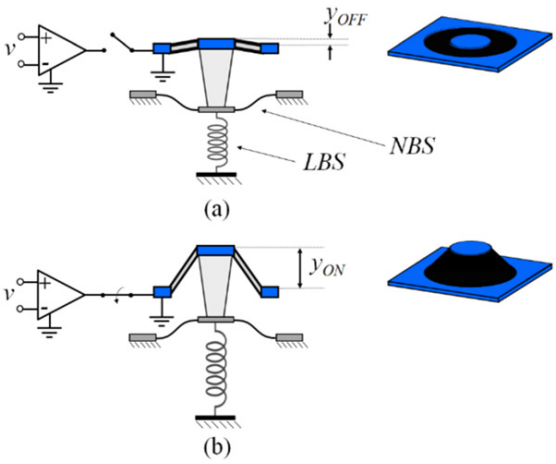

Figure 2. Circular DEA, voltage off (a) and on (b).

Table 1. DEA geometry in undeformed state.

Parameter	Value	Unit
Inner radius	6.25	(mm)
Outer radius	11	(mm)
Thickness	40	(μm)

2. DEA description and modeling

2.1. Actuator description

The actuator investigated in this work is based on the circular DE membrane shown in figure 1. The black ring represents the DE silicone material with compliant carbon-based electrodes screen-printed on the external surfaces. The inner circle and the outer frame (in blue) represent a passive plastic frame. When high voltage is applied to the electrodes, the resulting electrostatic compression induces a membrane squeezing which, due to the material incompressibility, produces the out-of-plane actuation shown in figure 2. The relevant geometrical parameters of the actuators in the undeformed state are reported in table 1.

As discussed in [21] an effective tradeoff between stroke and complexity can be obtained by a combination of a linear and a nonlinear bi-stable spring spring, denoted as LBS and NBS respectively. Despite the significant increase in stroke, the dynamic response of the NBS + LBS DEA is typically characterized by strong nonlinearities and hysteresis. However, such nonlinearities can be accurately modeled and compensated by means of model-based feedback control, allowing stable positioning in the entire actuation range [22].

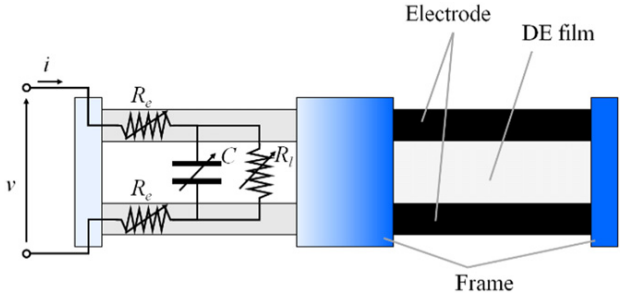

Figure 3. DEA equivalent electrical circuit.

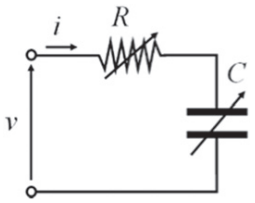

Figure 4. Leakage-free DEA equivalent circuit.

2.2. DEA electric model

The self-sensing requires the use of electrical measurements in order to reconstruct the DEA state of deformation. Several variables can be used to describe the DEA electrical response, e.g. voltage, current, charge. The charge measurement, however, is challenging due to the unavoidable drift produced by the leakage current. For this reason, in this work we use only the voltage v and current i to reconstruct the membrane geometry.

In order to describe the voltage–current response of the DEA, we adopt the electrical circuit shown in figure 3 [18]. The electrical model consists of a capacitor C connected in parallel with the leakage resistor R_l and in series with two resistors R_e taking into account the voltage drops on the electrodes. All these electrical parameters are assumed to vary according to the DEA deformation. We define the lumped series resistance R as

$$R(y) = 2R_e(y), \tag{1}$$

where y is the out-of-plane stroke. If the following condition holds

$$R_l(y) \gg 2R_e(y), \quad \forall\, y \tag{2}$$

we expect that the effects of leakage can be neglected at sufficiently high operating frequencies, without introducing a significant modeling error [23]. Considering the typical order of magnitude of the resistances, with R_l of the order of GΩ and R_e of the order of hundreds of kΩ [23], condition (2) holds. Therefore, the effects of the leakage can be neglected for self-sensing applications, in which we are mostly interested in the high-frequency electrical response. The resulting leakage-free model is the RC series circuit shown in figure 4. Note that the v–i relationship represents a high-pass filter. The model in figure 4 is described by the following

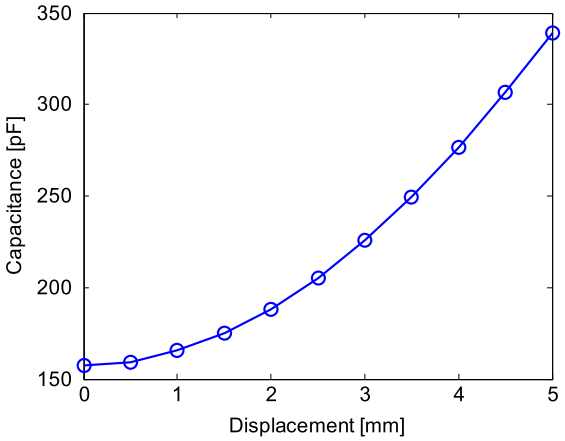

Figure 5. DEA capacitance versus displacement, experimental curve.

state-space realization

$$\begin{cases} \dfrac{\mathrm{d}}{\mathrm{d}t}q(t) = -\dfrac{1}{C(y)R(y)}q(t) + \dfrac{1}{R(y)}v(t) \\ i(t) = -\dfrac{1}{C(y)R(y)}q(t) + \dfrac{1}{R(y)}v(t) \end{cases}, \tag{3}$$

where the state variable q is the charge on the capacitor. The proposed model was proven to be accurate in describing the electrical response of the circular DEA, provided that an analytical expression is found for $C(y)$ and $R(y)$ [23].

3. Self-sensing closed loop control

Voltage and current measurements can be used as inputs for model (3) to estimate R and C, and then to reconstruct the displacement y using the relationship between electrical parameters and the geometry. The relationship between R and y, however, is typically hysteretic and frequency-dependent, while C is related to y in a monotonic way [19]. This is confirmed from the capacitance–displacement measured curve shown in figure 5, and performed with *Hameg*® LCR-bridge model HM8118. After these considerations, we conclude that the reconstruction of the deformation from the estimated capacitance is the most suitable for self-sensing in our case of study.

As highlighted in section 2.2, DEA have a high-pass voltage–current relationship. Therefore, the current resulting from a typical low-frequency actuation is not large enough to be accurately measured. To increase the measured current without affecting the actuation performance, we adopt the modulation approach proposed in [9]. An example of input voltage for performing self-sensing in DEA is shown in figure 6, and consists of a high-frequency, low-amplitude sensing signal which is superimposed to a low-frequency, high-amplitude actuation signal. The high-frequency sensing signal is then used to overcome the aforementioned limitation, as it provides a current response which is sufficiently large to be accurately measured, but it does not provide contribution to electromechanical actuation if its frequency is beyond the actuator mechanical bandwidth (typical values of mechanical bandwidth for the considered actuator are around 100 Hz).

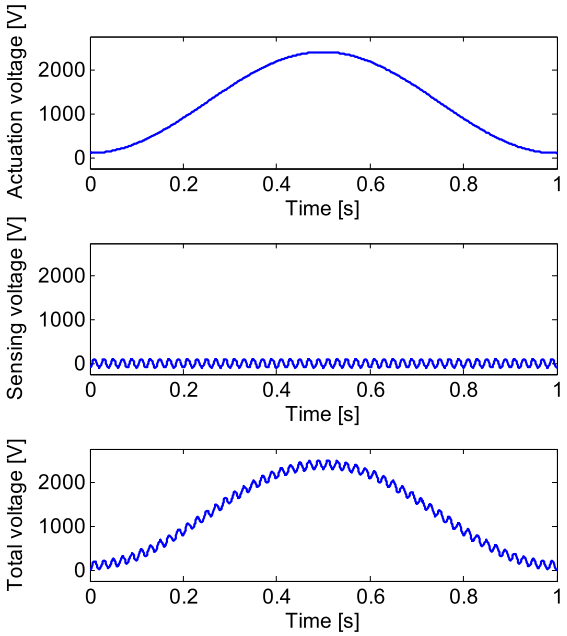

Figure 6. Actuation signal (upper), sensing signal (central) and complete self-sensing signal (lower).

3.1. Self-sensing algorithm

The self-sensing algorithm is based on the work presented in [19], and it is briefly summarized in this section. When the signal in figure 5 is applied to the DEA, voltage and current undergo fast changes due to the high-frequency input component (the low-frequency component is filtered from the electrical dynamics, and therefore its effects are not visible in the current response), while the capacitance and resistance undergo relatively slow changes at the same rate of the low-frequency voltage component. Therefore, if we acquire measurements with a sufficiently small sampling time T_s and restrict our attention to a relatively small time interval, we can assume that the time-varying behavior of C and R can be neglected, while the changes in v and i are non-negligible. If the derivative in (3) is approximated with forward Euler rule

$$\frac{\mathrm{d}}{\mathrm{d}t}q(t) \approx \frac{q(k+1) - q(k)}{T_s}, \tag{4}$$

where the variable k represents the discrete sampling time, we obtain the following difference equation

$$v(k) - v(k-1) = Ri(k) + \left(\frac{T_s}{C} - R\right)i(k-1). \tag{5}$$

It can be noted that equation (5) has the following Linear-In-Parameters structure

$$y(k) = \varphi(k)^T\theta, \tag{6}$$

with

$$y(k) = v(k) - v(k-1), \tag{7}$$

$$\varphi(k) = [\varphi_1(k) \quad \varphi_2(k)]^T = [i(k) \quad i(k-1)]^T, \tag{8}$$

$$\theta = [\theta_1 \quad \theta_2]^T = \left[R \quad \frac{T_s}{C} - R\right]^T. \tag{9}$$

The mathematical structure of (5) is particularly convenient as it opens up the possibility of estimating the parameters θ, i.e. R and C, in real-time by means of standard linear regression algorithms. As discussed in [19], a convenient choice is the use of recursive least squares (RLS) algorithm with exponential forgetting [24], given as follows

$$\begin{cases} \hat{\theta}(k) = \hat{\theta}(k-1) + K(k)(y(k) - \varphi^T(k)\hat{\theta}(k-1)) \\ K(k) = \dfrac{P(k-1)\varphi(k)}{1 + \varphi^T(k)P(k-1)\varphi(k)} \\ P(k) = \dfrac{1}{\mu}\left(P(k-1) - \dfrac{P(k-1)\varphi(k)\varphi^T(k)P(k-1)}{1 + \varphi^T(k)P(k-1)\varphi(k)}\right) \end{cases}. \tag{10}$$

The quantity $\hat{\theta}(k)$ represents the estimate of θ, i.e. capacitance and resistance, at time k, while $P(k)$ and $K(k)$ represent a covariance matrix and an observer gain matrix, respectively. The algorithm (10) can be tuned by choosing an appropriate forgetting factor μ in the range $0 < \mu \leqslant 1$. The value $\mu = 1$ is used when θ is constant, while a $\mu < 1$ allows the estimation of parameters which vary in time. The faster the variations of θ over time, the smaller should be the value of μ. However, lowering μ also reduces the filtering capabilities of the algorithm with respect to measurement noise. Therefore, the forgetting factor needs to be properly tuned to achieve the best trade-off between estimation velocity and noise propagation. This trade-off between velocity and noise filtering becomes even more crucial when operating in close loop.

Once a capacitance–deformation curve is initially calibrated, e.g. by means of polynomial interpolation, it can be inverted online during self-sensing operations.

Experimental evidence shows that the estimated capacitance is typically affected by high-frequency harmonic disturbances at multiples of the sensing signal frequency. In order to suppress these harmonics and improve significantly the self-sensing accuracy, some filtering strategies are suggested in [19]. The reader may refer to the aforementioned paper for further details.

3.2. Closed loop control

The displacement estimation can be used as feedback signal for a position control loop, which becomes in this case a sensorless scheme. A block diagram of the sensorless control architecture adopted in this work is shown in figure 7. The self-sensing block contains the algorithm described in section 3.1. Since we are mainly interested in comparing the closed loop performance of the sensor-based and self-sensing

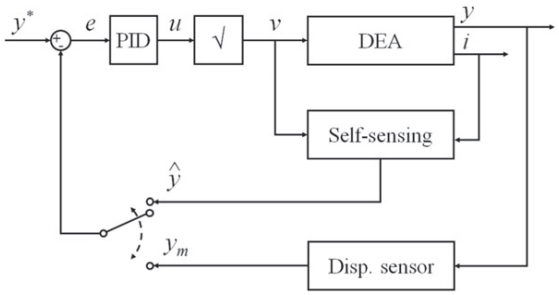

Figure 7. Closed loop control with displacement sensor/self-sensing switch block diagram.

based schemes, the only difference between the control architectures will be the source of the feedback signal (either the measured stroke, indicated with y_m, or the self-sensed stroke $\hat{y}$). This is represented by the switch in figure 7. We define the tracking error as

$$e(t) = y^*(t) - y(t), \tag{11}$$

where y can be either y_m or $\hat{y}$ depending on the experiment. The chosen control law has the form of a PID followed by a square root block as shown in figure 7 [15]. In particular, the PID output is defined as follows

$$u(t) = k_p e(t) + k_i \int_0^t e(\tau)d\tau + k_d \frac{d}{dt}e(t), \tag{12}$$

while the voltage v applied on the DEA is calculated from u as

$$v(t) = \sqrt{u(t)}. \tag{13}$$

The square root term was initially proposed in [15] to compensate the quadratic nonlinearity resulting from the electro-mechanical coupling equation. All the remaining material creep and nonlinearities, mainly due to the hyper-elasticity and bi-stability, can be effectively compensated with PID laws designed according to modern robust control tools, see e.g. [20, 22]. However, in this work we will concentrate the attention on hand-tuned PID laws to better focus on the possible loss of performance caused by the inaccuracies of sensorless feedback.

4. Experimental results

4.1. Experimental setup

The experimental setup used to validate the proposed self-sensing method consists of the DEA circular actuator with the NBS + LBS loading shown in figure 2 (max. applicable voltage 2.5 kV, max. out-of-plane displacement 5 mm). A *Zaber* T-NA08A25 linear actuator and a *Zaber* T-LA28A linear actuator used to modify the relative position of the two loading springs with respect to the DEA, allowing to tune the actuator performance. A *Trek* model 610E voltage amplifier (max. voltage 10 kV, bandwidth 1 kHz) is used to apply voltage to the DEA. As the bandwidth of the current monitor of the amplifier is not sufficiently large for our application, a

sensing circuit was designed on purpose for measuring the current absorbed by the DEA (range $\pm$ 500 μA). A *Keyence*™ LK-G37 laser displacement sensor is also used to obtain accurate displacement measurements (accuracy $\pm$ 150 nm), in order to validate the accuracy of the self-sensing estimation in both open- and closed-loop. A picture of the setup is shown in figure 8(a), with expanded views of the DEA (b) and the biasing springs (c).

The data acquisition, the control and the self-sensing algorithms are implemented in real-time in *LabVIEW* with an FPGA data acquisition system communicating with a host computer. All the measured variables (voltage, current, displacement) are acquired at a constant rate of 20 kHz. A sampling rate of 20 kHz is also selected for the self-sensing loop, while the position control algorithm updates the voltage signal at a rate of 5 kHz, as it is desirable that the sensing/self-sensing loops are operated at a non-slower rate than the control loop. Both algorithms are implemented on the FPGA by using a fixed-point representation with resolution of 24 bits. Since the input voltage v is constrained in the range [0, 2.5] kV to avoid electrical breakdown, the control law is implemented in an anti-windup configuration, with u limited within [0, 6.25] kV^2. Moreover, the analog PID defined by (12) to (13) is implemented in discrete time by adopting trapezoidal rule for the integral and finite differences for the derivative. A block diagram representation of the complete experimental setup is shown in figure 9.

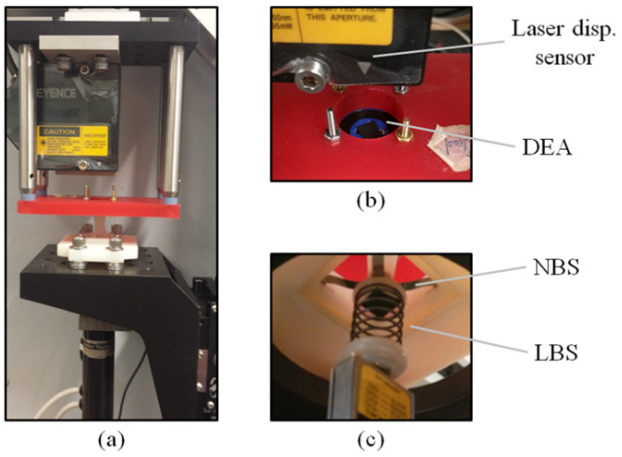

Figure 8. Full experimental setup (a), zoom on DEA (b) and zoom on biasing springs (c).

4.2. Open loop self-sensing tests

The first set of experiments aims at preliminary testing the proposed self-sensing methodology in open loop. In each test, the self-sensing algorithm is hand-tuned with a forgetting factor $\mu = 0.95$ and a high-frequency sensing signal consists of a 1 kHz, 75 V sinewave. A first calibration experiment is performed by applying a 0.1 Hz sinewave actuation voltage. The actuator displacement and the estimated capacitance are recorded with the laser displacement sensor and used to construct the displacement–capacitance curve with a third order interpolating polynomial. Subsequently, the calibrated curve is used to estimate the displacement during the actuation for three different actuation signals: an amplitude modulated square wave filtered with a first order low-pass filter (cut-off frequency of 3 Hz) and denoted as AMSQW, a 1 Hz sinewave and a sinesweep from 0 to 10 Hz.

The results are shown in figures 10–12. The displacement is measured by considering the completely undeformed DE membrane as zero reference level. Therefore, in each test the position starts from a non-zero value corresponding to the initial DEA deformation due to the biasing springs pre-compression. For all the experiments, the estimation error is never larger than the 4%. The error tends also to become smaller when the deformation is larger and occurs at a slower rate. This is an expected result, as the self-sensing algorithm is based on the assumption of constant resistance and capacitance, therefore the slower their variation the higher the estimation accuracy. Moreover, as the capacitance–displacement curve showed in figure 5 exhibits a parabolic trend, higher sensitivity can be obtained at larger deformations. The

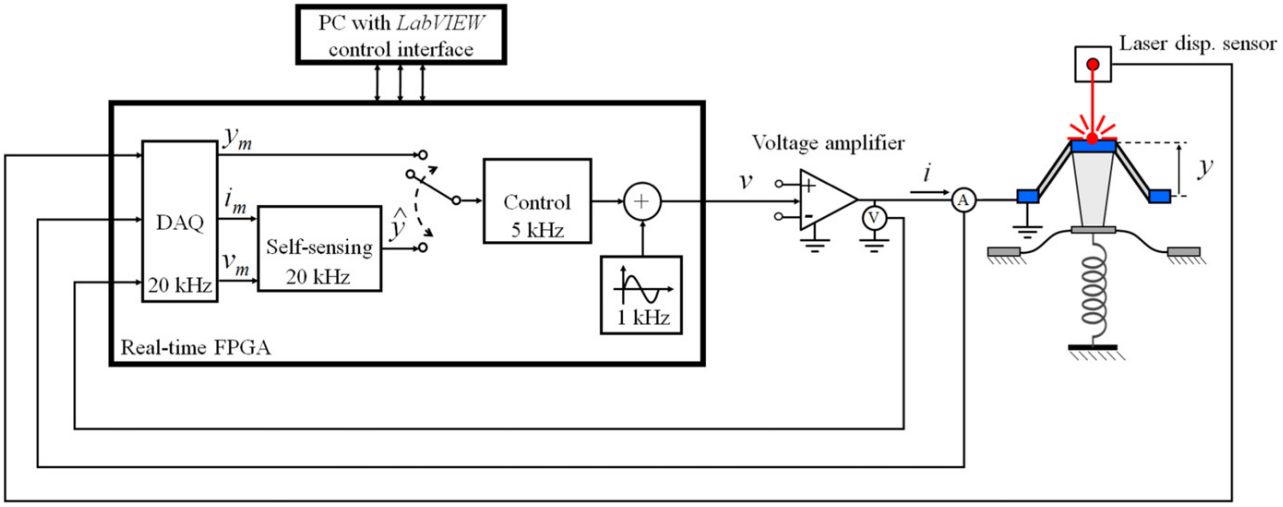

Figure 9. Block diagram representation of experimental setup used to test the sensorless control.

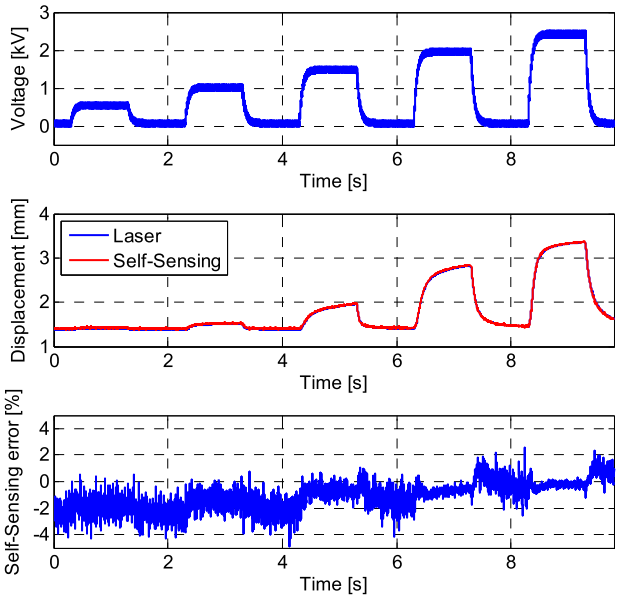

Figure 10. Self-sensing, AMSQW input, $\mu = 0.95$.

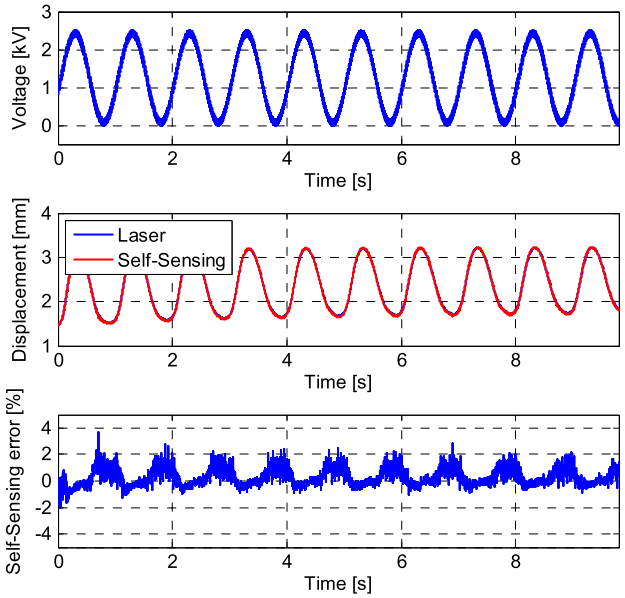

Figure 11. Self-sensing, 0.1 Hz sinewave input, $\mu = 0.95$.

experimental results clearly show the effects of the material creep, which leads to a slow drift of the position resulting from the application of a steady voltage. As the creep appears in both measured and self-sensed displacements, we can conclude that the capacitive based self-sensing is robust with respect to the material creep or, in other words, that the capacitance is instantaneously influenced by the material deformation and not on its mechanical stress.

Figure 13 shows the displacement–capacitance and the displacement–resistance curves estimated in each of the three experiments. The curves show that the displacement–capacitance relationship tends to remain consistent with the calibration curve, obtained with the 0.1 Hz sinusoidal signal. In case of sinesweep test (red curve), the estimated capacitance

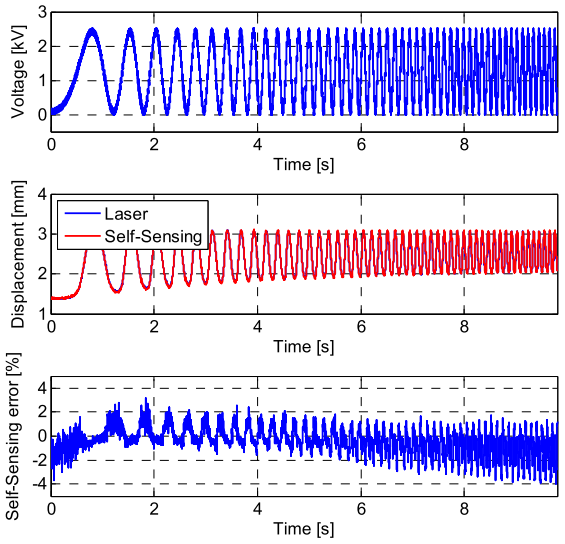

Figure 12. Self-sensing, 0–10 Hz sinesweep input, $\mu = 0.95$.

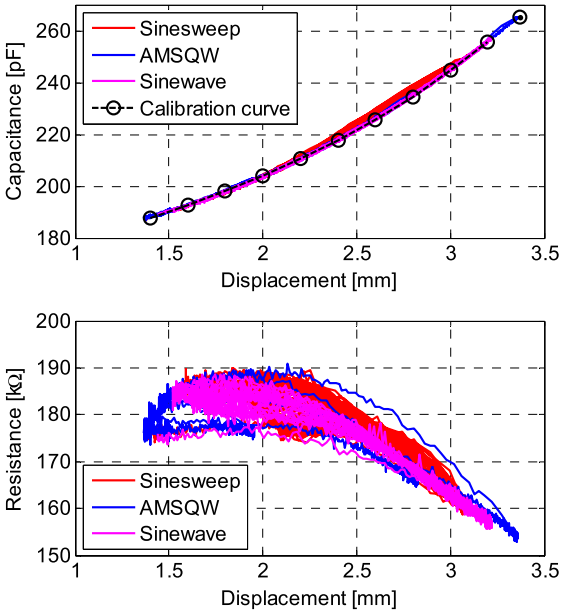

Figure 13. Estimated capacitance and resistance versus displacement for different tests, $\mu = 0.95$.

shows a larger deviation from the calibration curve, as the increase in mechanical frequency makes the estimation delay less negligible. The figure shows also that the resistance estimations are hysteretic and more affected by noise than capacitance. Nevertheless, the resistance data estimated for different tests are consistent with each other.

4.3. Sensorless closed loop control

The aim of the next set of experiments is to assess the effectiveness of the self-sensing based position control. By using again a 1 kHz, 75 V sensing sinewave, and choosing the forgetting factor equals to $\mu = 0.97$ (slightly higher than

Table 2. PID controller gains.

Controller	k_p	k_i	k_d
Controller 1	3	50	0
Controller 2	5	150	0
Controller 3	6	300	0

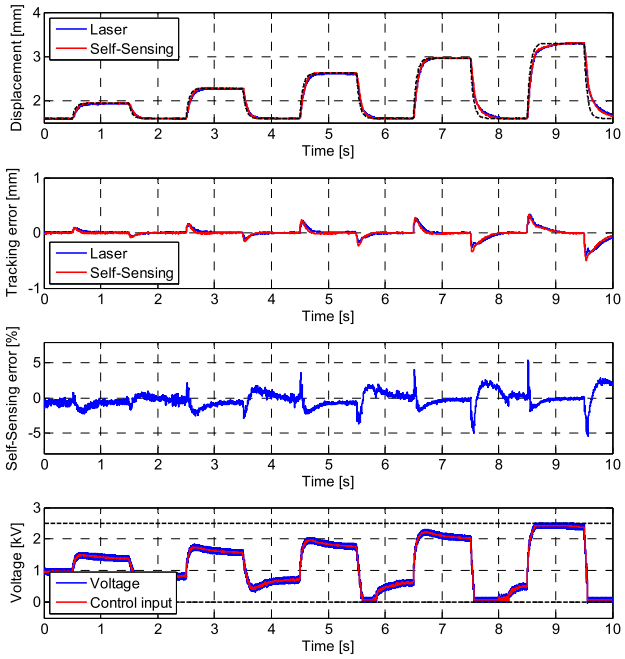

Figure 14. AMSQW reference, self-sensing feedback, controller 2, $\mu = 0.97$.

before in order to enhance the robustness with respect to noise), the PID gains are selected according to the tuning denoted as controller 2 in table 2. The results are shown in figure 14 for an AMSQW filtered with a first order low-pass filter with cut-off frequency of 3 Hz, in figure 15 for a 1 Hz sinewave and in figure 16 for a sinesweep from 0 to 5 Hz. Each figure shows both the measured and estimated displacement, the tracking error, the self-sensing estimation error and the input voltage. The closed loop behavior is satisfactory in each case, as the measured and self-sensed displacements are in good agreement with each other's.

In order to better quantify the degradation introduced by the self-sensing estimation in closed loop schemes, in the experiments shown hereafter the first half of each test implements the control law by using the laser displacement sensor feedback, and at $t = 5$ s the displacement feedback is switched to the self-sensing signal. The results are shown from figures 17 to 24. In particular, figures 17 to 19 show the performance for a step reference filtered with a first order low-pass filter with cut-off frequency of 3 Hz, with a fixed $\mu = 0.97$ and three different controller tunings, reported in table 2. Figure 20 shows the performance for Controller 1 and the same reference, but a different forgetting factor of $\mu = 0.99$ is used. Figures 21–24, instead, show the performance of similar experiments for a 0.2 Hz sinewave reference.

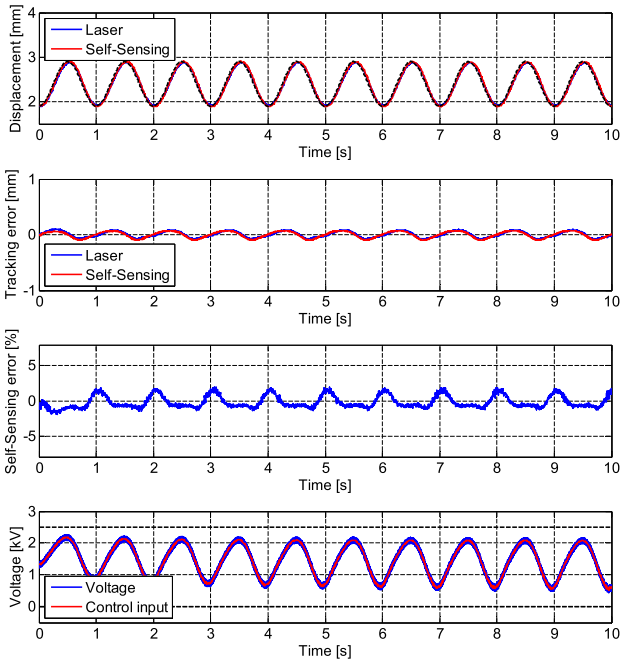

Figure 15. 1 Hz sinewave reference, self-sensing feedback, controller 2, $\mu = 0.97$.

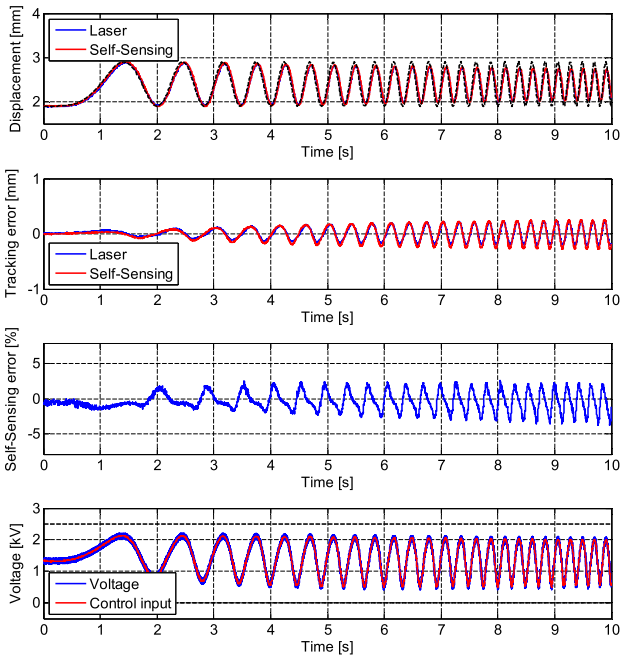

Figure 16. 0–5 Hz sinesweep reference, self-sensing feedback, controller 2, $\mu = 0.97$.

Finally, table 3 compares the performance of the experiments shown in figures 17–24 in terms of root mean square (rms) tracking error and peak (PK) tracking error calculated for both laser-based and self-sensing feedback, and rms and peak displacement estimation error. In each case, the rms and PK tracking errors are computed by considering the

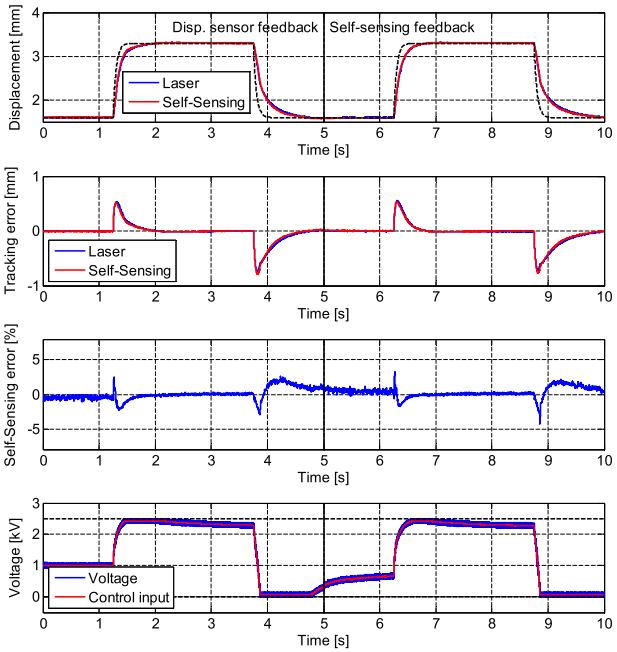

Figure 17. Step reference, disp. sensor feedback versus self-sensing feedback, controller 1, $\mu = 0.97$.

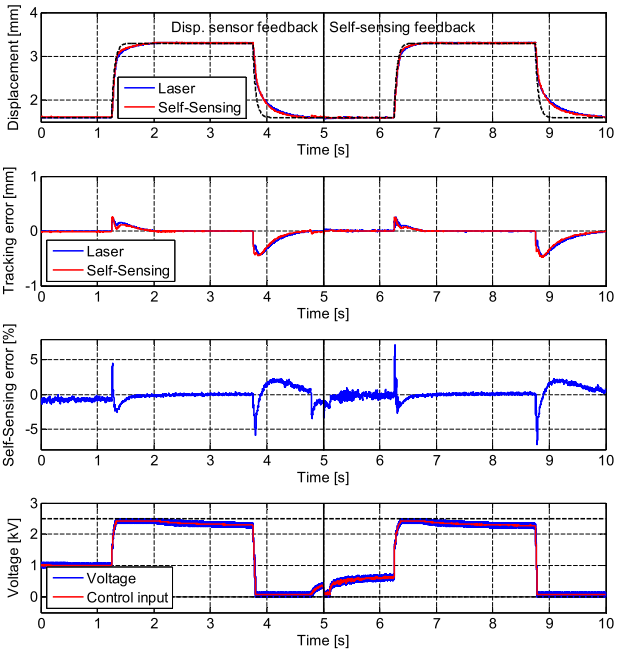

Figure 19. Step reference, disp. sensor feedback versus self-sensing feedback, controller 3, $\mu = 0.97$.

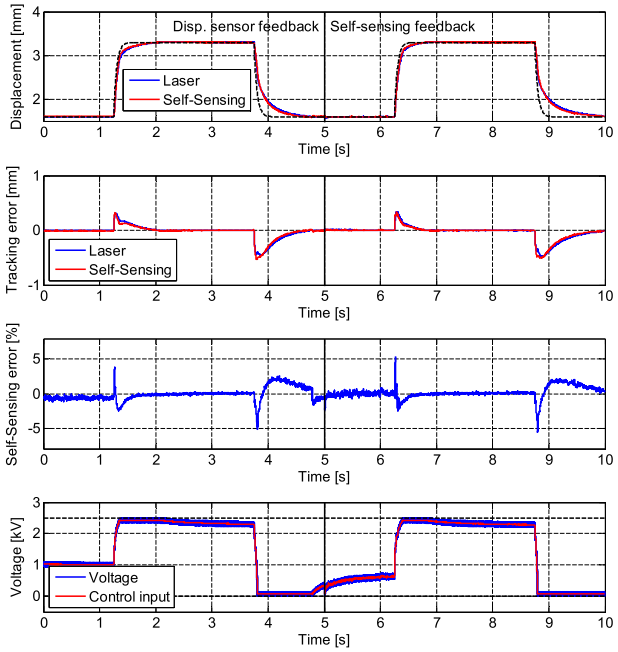

Figure 18. Step reference, disp. sensor feedback versus and self-sensing feedback, controller 2, $\mu = 0.97$.

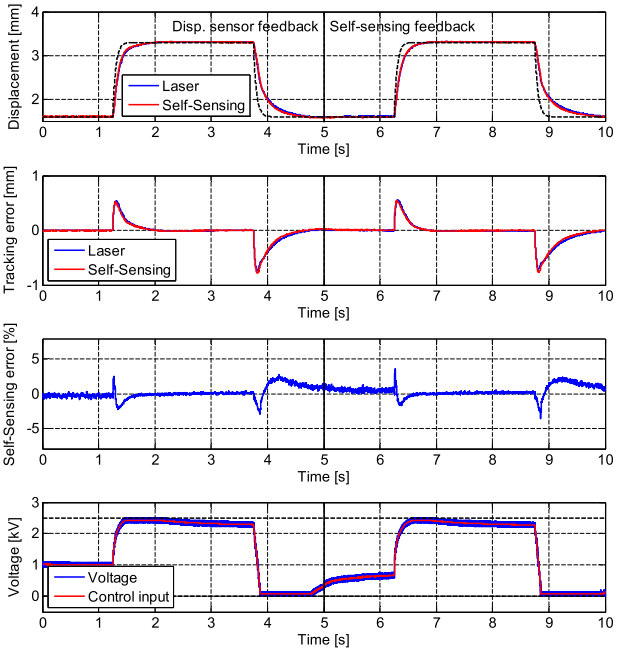

Figure 20. Step reference, disp. sensor feedback versus self-sensing feedback, controller 1, $\mu = 0.99$.

laser displacement sensor reading. For the step tests only, the peak errors at steady state (PK, SS) are also reported.

4.4. Discussion and performance analysis

The results obtained by using self-sensing based control in figures 14–16 show overall good performances.

The effects of the high-frequency signal injected for self-sensing are not visible in the output displacement, thus it does not affect significantly the closed loop behavior. Despite the strong nonlinearities of the actuator system, the proposed quasi-linear control architecture allows achieving a satisfactory closed loop response. By comparing voltage and displacement signals in figure 14, it can be noted that the system

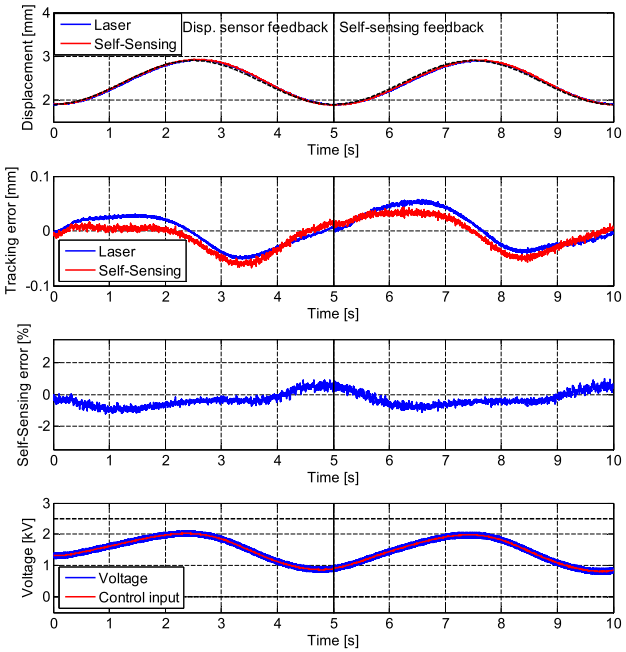

Figure 21. Sinewave reference, disp. sensor feedback versus self-sensing feedback, controller 1, $\mu = 0.97$.

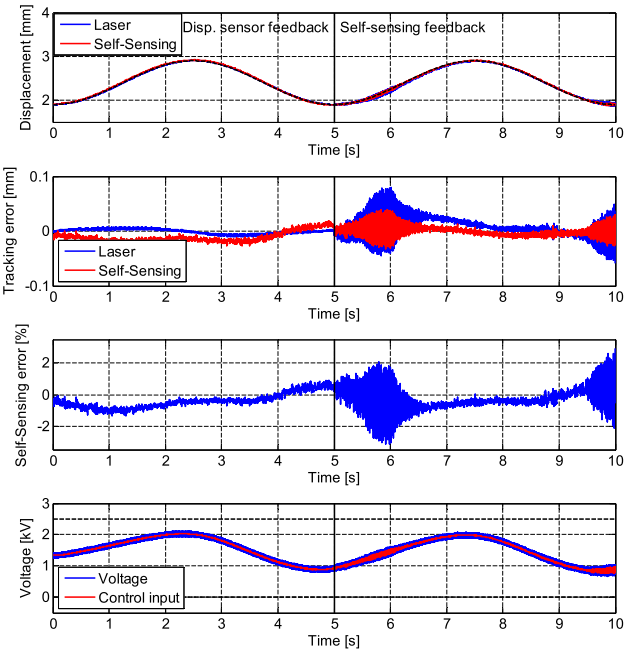

Figure 23. Sinewave reference, disp. sensor feedback versus self-sensing feedback, controller 3, $\mu = 0.97$.

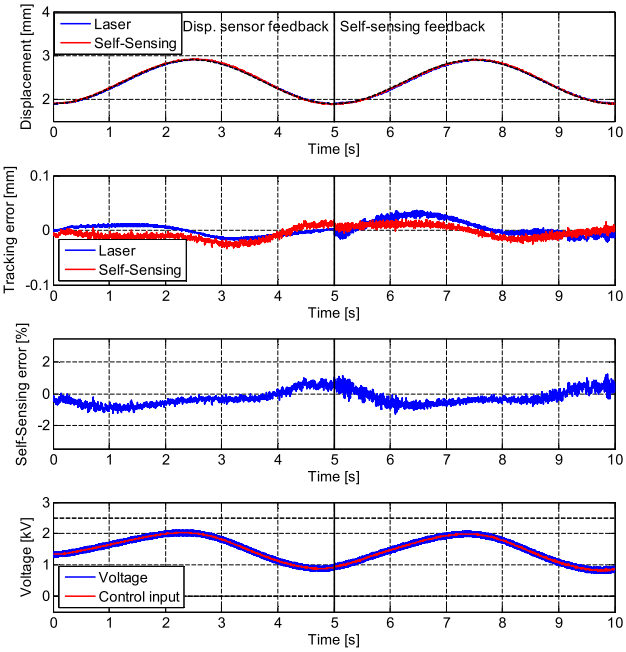

Figure 22. Sinewave reference, disp. sensor feedback versus self-sensing feedback, controller 2, $\mu = 0.97$.

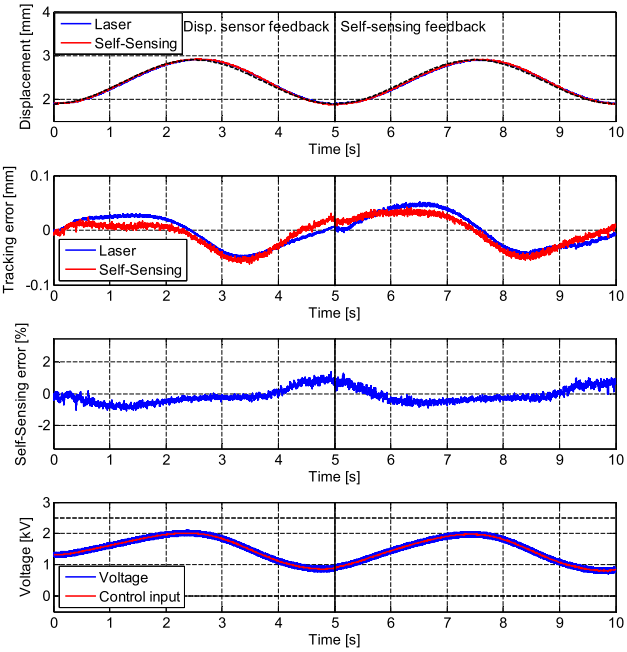

Figure 24. Sinewave reference, disp. sensor feedback versus self-sensing feedback, controller 1, $\mu = 0.99$.

response is delayed with respect to the voltage, presumably due to the material viscoelastic behavior. The effects of the viscoelasticity can be also clearly observed by inspecting the voltage imposed by the controller when the material is regulated at SS. In fact, in order to counteract the material creep observed in figure 10 and maintain a steady displacement, the controller needs to continuously decrease the actuation voltage. As no drift is observed in the self-sensing error, namely the error between measured and estimated displacement, we can conclude that the proposed sensorless control algorithm appears as an effective and robust strategy to compensate the material creep. Moreover, it can be observed that the self-sensing error tends to become relatively small at SS (less than 0.5%), thus ensuring accurate steady positioning. Overall, the peak values of the self-sensing error over the entire experiments are about 5% for the AMSQW,

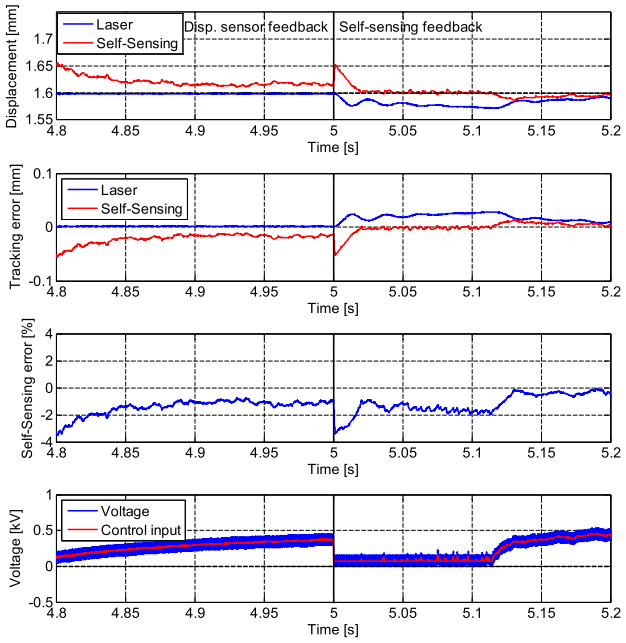

Figure 25. Zoom on step reference, disp. sensor feedback versus self-sensing feedback, controller 3, $\mu = 0.97$.

4% for the sinesweep and 2% for the sinewave. By inspecting figures 14 and 16, it can be noted that the self-sensing error is strongly related to the velocity and size of the signal, and becomes very close to zero when the deformation is slow-varying and large. This is in agreement with the considerations provided in section 4.2. The tracking error performance are satisfactory in each case, and show remarkable agreement between laser and self-sensing measurements. The tracking error is reasonably small for the AMSQW and the 1 Hz sinewave, but tends to increase with the input frequency in the case of sine sweep reference (figure 16). This is observed in the case of laser-based control as well [22], and it is due to the fact that the PID is not suitable for tracking fast-varying signals. In such case, more advanced control solutions are required in order to increase the tracking accuracy, but the investigation of these approaches goes beyond the scopes of this paper.

By comparing the left and right sides in figures 17–20 it can be observed that the closed loop performance and the estimation accuracy for the step reference are not significantly altered whether the feedback signal comes from the self-sensing rather than the laser displacement sensor. The figures show also the effects of the tuning parameters, namely the forgetting factor μ and the PID gains, on the closed loop system. No investigation of the effects of different sensing frequencies is performed in this paper, as this aspect was already analyzed in [19]. It can be observed that the performance of the sensorless scheme starts to slightly degrade as the gains are increased, as shown in figures 18–19, but still this change is relatively small and it does not affect the closed loop behavior significantly. This decrease of performance for increasing gains may be due to the overall delay introduced by the self-sensing in the feedback loop, caused by the combination of filters and RLS regression integrated in the self-sensing algorithm. The destabilizing effect of this delay becomes less negligible as the closed loop bandwidth is increased (and thus the resulting phase margin is decreased). Therefore, there are dynamic limitations on the achievable closed loop bandwidth in case the self-sensing algorithm is not fast enough. The comparison between figures 17 and 20, moreover, shows that the closed loop response is not significantly influenced by higher values of forgetting factor. Conversely, it is experimentally observed that the closed loop system becomes unstable if the forgetting factor is decreased (even if no results are shown in this paper). This may be due to several reasons, e.g. the increase of noise propagation or numerical instability due to the fixed-point implementation of the self-sensing algorithm, and certainly requires a more in-deep investigation. Figure 25 shows a zoom of the results in figure 19 on the time interval in which the displacement feedback is switched from the laser to the self-sensing. It can be observed that the control voltage generated in case of self-sensing feedback is slightly more nervous, as the self-sensing introduces additional noise which is inevitably propagated through the control loop. Consequently, a smaller oscillation can be observed in the SS displacement as well.

Similar results are also showed in figures 21–24, for a 0.2 sinewave reference. An oscillating, yet stable behavior can be observed in figure 23, confirming how the self-sensing scheme tends to affect the closed loop stability as the gains are increased. This oscillation is due to the fact that the controller is operating in a region where the DEA is open-loop unstable (because of the NBS), and the large controller gains in conjunction with the system local instability and the delay introduced by the self-sensing result in a closed-loop local instability. This instability appears systematically when the actuator position is about 2 mm, and only in case of self-sensing based control. Therefore, the closed loop bandwidth that can be achieved with self-sensing is further penalized in case the dynamics of the DEA presents strong nonlinearities such as bi-stability. Nevertheless, if the gains are tuned to more reasonable values, good performance and stable positioning can be still achieved even in case of bi-stable DEA, as confirmed by other reported plots. In general, this problem can be potentially addressed by taking into account of the dynamics of the self-sensing during the controller design, even if no methodologies to address this problem have been presented so far in case of DEA systems.

Finally, the inspection of table 3 confirms the results previously discussed. The SS accuracy achieved with self-sensing in case of step signals is always below 10.5 μm, while in case of sensor-based feedback is below 5.5 μm, for a stroke of 1.7 mm, and the SS self-sensing error is always not larger than 0.4%. The tracking performance in the case of sinewaves tends to degrade when the gains are increased, as the peak error of self-sensing based control shows comparable values for smaller gains, and tends to diverge in case of the faster controller. Nevertheless, the estimation accuracy is still relatively high (less than 1.5% in most of the cases). Comparing the performance in terms of rms error rather than peak error provides little if no degradation in performance in most of the

Table 3. Laser based feedback versus self-sensing based feedback, performance comparison.

Experiment shown in	Tracking error, sensor			Tracking error, self-sensing			Displacement estimation error		
	rms (μm)	PK (μm)	PK, SS (μm)	rms (μm)	PK (μm)	PK, SS (μm)	rms (%)	PK (%)	PK, SS (%)
Figure 17	168	735	5.25	176	713	9.45	0.82	4.25	0.35
Figure 18	118	458	3.45	127	484	8.25	0.91	5.57	0.32
Figure 19	106	432	1.80	115	461	10.2	1.00	7.28	0.38
Figure 20	197	735	5.40	176	714	10.4	0.87	3.65	0.37
Figure 21	26.4	51.2	—	32.4	57.9	—	0.55	1.24	—
Figure 22	8.72	18	—	15.8	35.9	—	0.53	1.31	—
Figure 23	4.36	9.90	—	21.0	80.3	—	0.73	3.13	—
Figure 24	26.1	51.0	—	49.2	31.4	—	0.49	1.38	—

cases, for both steps and sinewave references, and for both tracking and self-sensing errors. Therefore, we can conclude that the overall behavior of the self-sensing based control is satisfactory.

5. Conclusions

In this work, it was experimentally proven that the proposed self-sensing methodology can be successfully used in closed loop operation. The degradation of performance caused by the sensorless feedback was deeply investigated by means of numerous experiments. It was observed that the decrease in performance introduced by the self-sensing is almost negligible for slower closed loop bandwidths, and tends to increase for higher controller gains. The SS performance in case of slow-varying signals is generally high, showing a peak tracking error always smaller than 10.5 μm, against 5.5 μm obtained in case of sensor-base feedback, on an actuation stroke of about 1.7 mm. The resulting accuracy is satisfactory in many micropositioning applications. Compensation of the position drift due to the material creep is also effectively achieved by means of self-sensing feedback.

It can be noted that the self-sensing still performs satisfactorily even if the capacitance estimation requires the derivative of the control voltage (see (5)). The noise amplification produced by this derivative tends to become more significant when the self-sensing operates in closed loop, especially for larger controller gains which tend to amplify even more such effects. Therefore, further developments of the current work will be devoted to investigate more sophisticated self-sensing methodologies which allow to eliminate such dependency on the voltage derivative. The analytical investigation of the effects of the self-sensing in the control loop, and the joint optimization of the controller and the self-sensing parameters are other interesting directions for further research.

Acknowledgments

The authors would like to acknowledge the support of Parker Hannifin™, BioCare Business Unit.

References

[1] Carpi F, Rossi D D, Kornbluh R, Pelrine R and Sommer-Larsen P 2008 *Dielectric Elastomers as Electromechanical Transducers* (Amsterdam: Elsevier)
[2] Loverich J J, Kanno I and Kotera H 2006 Concepts for a new class of all-polymer micropumps *Lab. Chip* **6** 1147–54
[3] Giousouf M and Kovacs G 2013 Dielectric elastomer actuators used for pneumatic valve technology *Smart Mater. Struct.* **22** 104010
[4] Plante J S 2006 Dielectric elastomer actuators for binary robotics and mechatronics *PhD Dissertation* Dept. of Mechanical Engineering, Massachusetts Institute of Technology
[5] Jordan G, McCarthy D N, Schlepple N, Krißler J, Schröder H and Kofod G 2011 Actuated micro-optical submount using a dielectric elastomer actuator *IEEE/ASME Trans. Mechatronics* **16** 98–102
[6] Anderson I A, Gisby T A, McKay T G, O'Brien B M and Calius E P 2012 Multi-functional dielectric elastomer artificial muscles for soft and smart machines *J. Appl. Phys.* **112** 041101
[7] Janocha H 2013 *Unkonventionelle Aktoren—Eine Einfuehrung* 2nd edn (München: Oldenbourg)
[8] Chuc N H, Thuy D V, Park Jm K D, Koo J, Lee Y, Nam J-D and Choi H R 2008 A dielectric elastomer actuator with self-sensing capability *15th Int. Symp. on: Smart Structures and Materials & Nondestructive Evaluation and Health Monitoring* p 69270V
[9] Jung J, Kim K J and Choi H R 2008 A self-sensing dielectric elastomer actuator *Sensors Actuators* A **143** 343–51
[10] Matysek M, Haus H, Moessinger H, Brokken D, Lotz P and Schlaak H F 2011 Combined driving and sensing circuitry for dielectric elastomer actuators in mobile applications *Proc. SPIE* 797612
[11] Gisby T A, O'Brien M and Anderson I A 2013 Self sensing feedback for dielectric elastomer actuators *Appl. Phys. Lett.* **102** 193703
[12] Hoffstadt T, Griese M and Maas J 2014 Online identification algorithms for integrated dielectric electro-active polymer sensors and self-sensing concepts *Smart Mater. Struct.* **23** 104007
[13] Sarban R and Jones R W 2012 Physical model-based active vibration control using a dielectric elastomer actuator *J. Intell. Mater. Syst. Struct.* **23** 473–83
[14] Wilson E D, Assaf T, Pearson M J, Rossiter J M, Anderson S R and Porrill J 2013 *Bioinspired Adaptive Control for Artificial Muscles Biomimetic and Biohybrid Systems* (Berlin: Springer) pp 311–22